

Optical Engineering

OpticalEngineering.SPIEDigitalLibrary.org

Parallel guidance endoscopic optical coherence tomography system for internal diagnosis through active cannulas

Suhyeon Gim
Hyowon Moon
Hyun-Joon Shin
Deukhee Lee
Sungchul Kang
Keri Kim

Parallel guidance endoscopic optical coherence tomography system for internal diagnosis through active cannulas

Suhyeon Gim,^{a,b} Hyowon Moon,^b Hyun-Joon Shin,^{b,c} Deukhee Lee,^{b,c} Sungchul Kang,^{b,d} and Keri Kim^{b,c,*}

^aInstitut Pascal/University Blaise Pascal-UMR CNRS 6602, Aubière cedex 63171, France

^bKorea Institute of Science and Technology, Center for Bionics, Hwarangno 14-gil 5, Seoul 136-791, Republic of Korea

^cKorea University of Science and Technology, Department of Biomedical Engineering, 217 Gajeong-ro Yuseong-gu, Daejeon 305-350, Republic of Korea

^dKorea University of Science and Technology, Department of HCI and Robotics, 217 Gajeong-ro Yuseong-gu, Daejeon 305-350, Republic of Korea

Abstract. A parallel guidance endoscopic optical coherence tomography (OCT) system is proposed for minimally invasive internal inspection of inner organs or complex structures for diagnosis. The system is maneuvered to access the target using an active cannulas' steerable structures. The integration of a specially designed linkage device with the developed system allows the OCT endoscope to scan with enhanced signal-collective performance, while maintaining its tip at a constant distance from the target, as well as expanding the scanning range. The proposed system is integrated with flexible active cannulas, and this prototype is used for testing. The test results show that the device reliably performs for biological samples. Thus, it could be implemented for various types of noninvasive diagnoses in situations involving small entrances or crooked passage to a target. © The Authors. Published by SPIE under a Creative Commons Attribution 3.0 Unported License. Distribution or reproduction of this work in whole or in part requires full attribution of the original publication, including its DOI. [DOI: 10.1117/1.OE.53.8.084105]

Keywords: optical coherence tomography; active cannulas; parallel guidance; minimally invasive surgery; internal diagnostics.

Paper 140282 received Feb. 18, 2014; revised manuscript received Jul. 1, 2014; accepted for publication Jul. 8, 2014; published online Aug. 7, 2014.

1 Introduction

Optical coherence tomography (OCT) has been developed for over a decade. Currently, it is widely used for microscale diagnosis and therapy due to the method's specific advantages such as high depth and transverse resolution and its especially nondestructive nature.¹ There are many types of OCT systems that differ according to the signal processing in terms of time and frequency, beam forming, guidance, and application fields. Endoscopic OCT is used for the high-resolution diagnosis and therapy of internal organ systems in fields such as cardiology, urology, dermatology, ophthalmology, gastroenterology, cochlear implants, and for obtaining biopsies of various types of cancers.²⁻⁴ The noticeable disadvantages of endoscopic OCT are the limited scanning depth for dispersed media and a small lateral scanning range. To overcome these limitations, many bi-directional improvements have been proposed for OCT probe guidance; these include side imaging and a forward imaging scope. The side imaging technique expands the scanning range through circumferential motion in conjunction with longitudinal translation, which is effective for inspection around small cylindrical passages such as blood vessels.⁵ An optical fiber with a scope probe is mainly actuated through base rotation, and its rotational acquisition combined with its longitudinal motion allows for the collection of inter diagnostic information around the outer walls.⁶ In contrast to side imaging, the forward imaging method emits a laser beam in the forward direction and controls beam forming using a microelectromechanical systems (MEMS) mirror or some active material. This microendoscope is used for scanning forward areas when directed toward a target

surface. Different types of forward imaging OCT systems are described in Ref. 5.

Even though a microendoscope can acquire images on flat surfaces which are not accessible by the side imaging scope, it has a narrow field of view. Specifically, because the MEMS mirror or the cantilever-type guide is in the endoscopic tube, the scanning range is limited by its encircling tube. For resolving this challenging issue, single mode fiber has been introduced for pose control of OCT probes,⁷ and dexterous robotics manipulation has been used in OCT guidance for intraocular surgery.⁸ Interested readers are encouraged to refer to Refs. 5, 9, and 10 for well-summarized literatures about the various endoscopic OCTs, including different probe designs, typical parameters, and their limitations.

The functions and specifications of OCT systems depend on their applications. Surgery for installing cochlear implants is one of the most challenging procedures for which the OCT system is of significant importance.¹¹⁻¹⁴ In this paper, a parallel guidance OCT system is proposed for inter diagnostics with active cannulas. It could act as a solution in situations where the entrance passage to a target is narrow and crooked, and the manipulation of a rigid instrument could damage the surrounding structures, i.e., cochlear implant intervention. These and similar situations are currently handled using flexible instruments having limited configurations. The OCT system is designed to be integrated into and controlled by active cannulas for minimally invasive endoscopic diagnosis.

The remainder of this work is organized as follows. In Sec. 2, the OCT system and its integration with active cannulas are described. In Sec. 3, the parallel guide system is presented with some demonstrative explanation, and finally, the experimental results are presented with conclusions and an outline of future work.

*Address all correspondence to: Keri Kim, E-mail: jazzpian@kist.re.kr

2 Endoscopic Optical Coherence Tomography System for Biological Diagnosis

OCT is a noninvasive optical imaging technique that is generally used for biological tissues.⁶ By using a low-coherence optical interferometric method, OCT images of micrometer scale resolution can be obtained. This resolution is considerably higher than those of magnetic resonance imaging and other noninvasive imaging methods. Thus, OCT has been widely used for obtaining two- or three-dimensional images of tissues.¹⁴ However, applications of OCT are limited because the maximum scan depth of conventional OCTs is usually less than a few millimeters. An enhanced type of OCT has overcome this limitation by using a MEMS-VCSEL¹⁵ types swept source, which can image a few tens of millimeters. For solving the problem of the small range of depth, an endoscopic OCT was developed and studied.¹⁶ It uses a flexible optical fiber with a small-diameter gradient-index (GRIN) lens. Thus, this system could be integrated with catheters or insertion needles for image acquisition from biological targets located deep within the body.

Figure 1 shows the implemented OCT system where 1(a) is a fundamental OCT system and 1(b) is the integrated endoscopic system with active cannulas. In Fig. 1(b), the reference arm is noted by **R** and the sample arm is noted by **S**; these are implemented into the inner tube of the active cannulas for the probe to be feedback-controlled by a control computer. The system uses spectral-domain OCT (SD-OCT), which affords better detection sensitivity and faster image scanning rates than conventional time-domain OCT. It uses a broadband light as a light source and does not

need a scanning reference mirror. In this study, a superluminescent diode (SLD) with a center wavelength of 780 nm and full width at half maximum (FWHM) bandwidth of 50 nm was used as the light source. The center wavelength was selected as 780 nm because the absorption coefficient of water increases as the wavelength increases in the near-infrared region, and those of hemoglobin and melanin are too high in the visible region.¹⁷ The light from the SLD is passed through a 2×2 coupler and is divided as 50:50. Half of the light is directed at a retroreflector, which is used as a reference mirror, and half passes through the GRIN lens on its way to the sample. The diameter of the GRIN lens was 1 mm, which is small enough to be inserted through an active cannula. The length and working distance of the GRIN lens were 2.68 and 5076 nm, respectively. The axial resolution of the system is $6.5 \mu\text{m}$ in air and $4.9 \mu\text{m}$ in water, and its scan depth is 6 mm in air and 4.5 mm in water. The system's lateral resolution is $23.7 \mu\text{m}$ in air and $31.5 \mu\text{m}$ in water.

Light reflected from the sample and the retroreflector (reference mirror) interfere in the coupler and are detected by a line scan charge coupled device camera having a resolution of 2048 pixels after passing through a diffraction grating and a collimating lens. The transmission grating (WasatchPhotonics, Logan, Utah, 1200 1/mm @840 nm) and triplet collimators (Thorlabs, Newton, New Jersey, F220APC-780) were used for the experiment.

The line scan camera acts as a spectrometer because the two light streams are spectrally decomposed during their passage through the grating. The data obtained by the camera were sampled with equal wavelength increases and interpolated into k -space before Fourier transformation ($k = 2\pi/\lambda$). The Fourier-transformed data represent the axial depth image of one point. The theoretical sensitivity of the system is 115.2 dB and its imaging speed is 50 A-scan/sec, where the scanning rate is set up with the proposed parallel moving speed on the probe guidance at the computation speed for Fourier image processing, and the operational conditions determine the imaging quality with resolution. A few system specifications are summarized in Table 1.

3 Guidance and Control System

3.1 Active Cannulas System

The proposed endoscopic OCT system is implemented with active cannulas, which act as flexible steerable manipulators

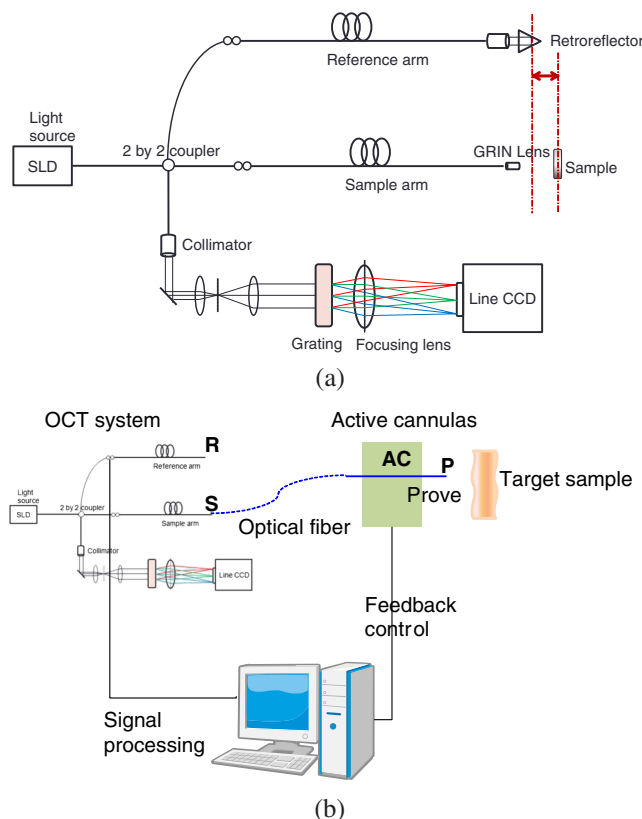


Fig. 1 Schematic diagram of OCT system: (a) SD-OCT, (b) integrated OCT system.

Table 1 OCT system specifications.

Specifications	Distance
Wavelength	780 nm
FWHM	50 nm
Axial resolution	$5.35 \mu\text{m}$
Lateral resolution	$23.7 \mu\text{m}$
Depth of focus	1.8 mm
Scan depth	4.056 mm
Working distance	5.5 mm

that can guide the endoscope toward the target through a small passage. Active cannulas have attracted attention in the field of surgical robotics and among device manufacturers because of their steerability and flexible structure. They can access a target through small, crooked entrances, or natural orifices. Active cannulas consist of consecutive tubes of reduced diameters. Each tube has straight and curved sections from its base.

Active cannulas have been developed and clinically validated with a composition of successive telescopic, concentric, precurved, and superelastic tubes for in-depth analysis from mechanical, geometric, and systemic viewpoints. They are intended for various types of small-scale laparoscopic surgeries such as endonasal skull base surgery, brain surgery, blood vessel surgery, and reaching lesions in the peripheral lung.¹⁸ Active cannulas exhibit a novel and delicate motion performance at the millimeter scale due to enhanced dexterity of the end-effector because of the telescopically interlinked structure. This structure is realized by following a methodology of efficient kinematics computations, affording individual tube rotation and translation for controlling the tip's pose. For satisfying microsurgical requirements while extending the device's applicability to cochlear implant operations, especially for scanning the inner surface to find an intrusion point into the cochlea, an OCT integrated with active cannulas is proposed and implemented in this study. The objective of the developed active cannulas-guided OCT system is to be as minimally invasive as possible when inside the body.

However, the OCT system with active cannulas has some limitations in terms of parallel motion of its end-effector, i.e., the scope cannot have a sufficient parallel scanning motion without a large motion of the outer tubes. In this case, the entrance or passage could be damaged or the scope could vibrate with the active cannula's bodies, thus introducing undesirable noise into the scanning result. Furthermore, the existence of nonlinearity and critical limits known as bifurcation¹⁹ could lead to unexpected pose errors, which is not desirable for microscale measurements in narrow spaces. The use of a cantilever-type probe could increase the scanning range on the frontal surface. However, probe orientation, which determines the beam direction, is varied per scan. Furthermore, it is difficult to determine its orientation of the tip because of the complex nonlinear characteristics of the interaction between the actuation force and the deflection. If accurate probe orientation during a scan is not known, the result does not reflect the actual state. This problem is significant when measuring flat surfaces. When the target surface is flat, the reflective signals weaken as the deflection angle increases. In other words, a parallel guide for the OCT probe is required for obtaining clear images through expansion of the lateral movement range. To this end, we propose an endoscopic OCT system which is guided in parallel for solving the abovementioned difficulties.

The active cannulas are made of a shape memory alloy (Nitinol) tubes manufactured by Nitinol Devices & Components Inc., Fremont, California, and they are controlled by a sophisticated control system. The active cannulas or steerable manipulators have multiple curved sections in the longitudinal direction; the shapes of these sections can be restored up to deformation. Each constructive tube has straight or precurved regions which are manufactured by

Table 2 Active cannulas tubes specifications. [mm]

Tube	D_o	D_i	t	l_s	l_c	l_z	k
Outer	3.000	2.820	0.180	100.0	0	0.872	5.5
Inner	2.363	2.130	0.233	80.0	20	0.520	8.4

heating at over 500°C for 30 min in a brass mold, followed by tempering in cold water. The brass mold for the thermal process is elaborately designed to ensure that the tubes have moderate stiffness and flexibility. In the process, there is much stress on maintaining the increasing and cooling speeds of the temperature for the object; hence, the mold has a specific design shape. It could be important in clinical aspects to specify these parameters on the tubes in the active cannulas as shown in Table 2.

In Table 2, two tubes have differences in their outer/inner diameters (D_o/D_i) with a thickness (t), a straight length (l_s), curved lengths (l_c), area moments of inertia (I_z), and curvatures (k) where all values are denoted based on [mm]-dimensions. The inner diameter D_i for the inner tube is important so as to allow the OCT probe to pass through the inside of the tube; the curvature with a curved length of the tube is a clinical design parameter to inspect or access the target for the OCT guidance. This parameter setup was designed with its major clinical target a cochlear implant, but it could be differentiated depending on its clinical purposes.

The integrated robot hardware system has dimensions of 80 × 70 × 400 mm in, width × height × length, as shown in Fig. 2.

The system has been specifically designed for control using active cannulas. It weighs less than 1.5 kg, has a portable size, and offers other facilities such as a power transducer and accessory cables. The control system is composed of four DC motors with two cannula tubes, two motors of which take part in the translational motion and the others in the rotational motion of each cannula tube. The inner tube fixes the probe inside and the outer tube changes the curvature of the inner tube by curvature overlapping by relative translation. The rotation of the probe pose is also performed by rotational motions of both tubes. With two-tube motions, the resultant workspace on the probe position presents a conic volume¹⁸ for covering a wider

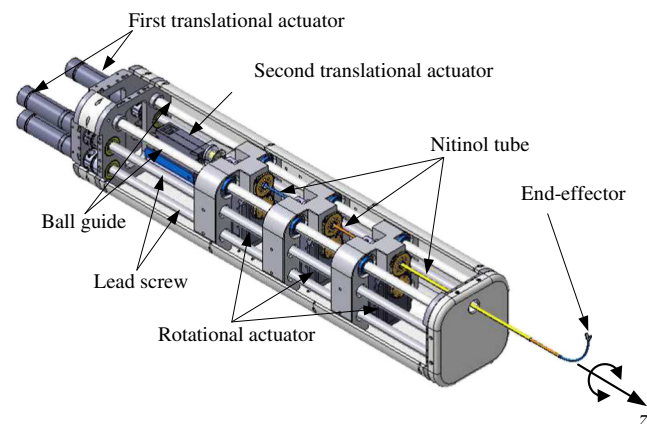


Fig. 2 Active cannulas system.

diagnostic space than a straight probe. All motors are controlled using a Maxon (Postfach, Switzerland) EPOS2 driver connected to a PC with a 1 Mbps CAN communication channel. The control module is written in C++.

Given that one of the possible applications is cochlear implant installation, where the surface of the inner organ has a circular patch with a diameter less than 0.5 cm, two active cannulas are used for achieving efficient scanning performance in the range. In the two-tube system, the parallel guidance OCT scope is implemented on the tip-end of the inner tube, and the pose of the guidance system is controlled by translation and rotation, or any combination thereof, of each tube. Even though there are some useful scope pose compensation algorithms^{17,20} for measurement images, it is important to achieve fine control of the probe's pose for acquiring an analyzable and diagnostically significant image quality. The end-effector pose is determined through kinematic calculations and is achieved by controlling the translation and rotation of the telescopic tubes, as described in Refs. 18, 19, 21, 22, and 23. Although a positional error of less than 1 mm has been achieved in real experiments, it is difficult to improve the system's accuracy. In addition, it is difficult to control using real-time pose sensing feedback because acquisition of accurate pose information with the existing sensors is difficult. Furthermore, during the translational motion of each tube, there is internal sliding contact between the tubes' walls, which leads to nonlinear pose errors of the end-effector. Therefore, a diagnostic system based only on active cannulas is insufficient for microscale measurement.

Orientation control is a major issue in measurement. Probe orientation is more important because it is directly related to the direction of the OCT probe, where its reflective ratio is also affected by the target surface texture. Because the precurved region of each tube could be changed under some experimental conditions and the analytical model is characterized by fundamental uncertainty errors of the real model, as well as those related to repetitive control accuracy with the OCT scanning sampling, the calibration of tip orientation is indispensable. For that purpose, visible rays are transmitted through the optical fiber installed for OCT, and their arrival point on the focusing plane is marked on a graph paper slide and measured with geometrical considerations. After calibration, a pose accuracy of under 0.5 mm and 1° was achieved. Note that this procedure is performed on the system operation level, not on the imaging level to enhance the pose control accuracy of active cannulas, such that the probe accesses the target sample.

3.2 Parallel Guidance System

The active cannulas are used for expanding the scanning range on a target surface that offers a limited motion configuration because of its hidden location, which may require passage through long, crooked openings. Thus, the end-effector, which is the end of the manipulator, could be used for obtaining OCT images of complex electronic devices or diagnosis of an inner organ in a noninvasive manner.

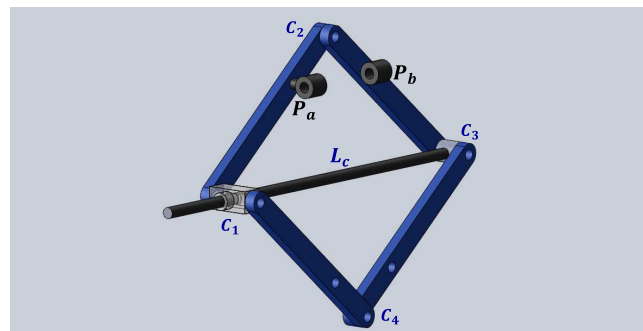
Even if the positions of the active cannulas are controlled with three consecutive tubes, the end-effector orientation is not easily or accurately manipulated because the system has its own critical zone and has nonlinearities such as bifurcation. With respect to the OCT performance, the parallelism of

the scope with the target surface is the most important function. Therefore, the active cannulas are required to use an additional system for ensuring parallel probe scanning motion.

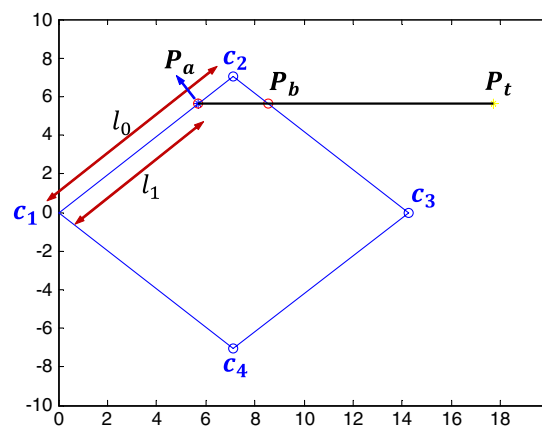
The OCT probe is equipped with the parallel guidance system as shown in the following figure.

In Fig. 3, the proposed parallel guidance system is shown, where (a) shows a three-dimensional (3-D) view with some notations, and (b) shows the geometric schematic. In Fig. 3(a), there are four joints from C_1 to C_4 connecting neighboring linkages. The probe is loaded at holders P_a and P_b , and each holder is allowed to rotate to the linkage bars. The control link L_c plays the important role of pulling or drawing the joint C_3 through C_1 , and it is connected to the actuator in the active cannulas system. Here, the control link is superelastic, and it can exert forces in both directions along the flexible cannulas' structure. The left side of the joint C_1 is located inside the tube of the active cannulas. In Fig. 3(b), the OCT probe is represented by positions P_a , P_b , and P_t , where the tip of the probe is denoted by the subscript t . There are some geometrical relations according to the length of the control link L_c .

When the length of a linkage bar is l_0 and the length from C_1 to P_a is l_1 , it is assumed that by varying dl of the control link, the angle of the linkage bar on the horizontal plane, θ , varies from θ_1 to θ_2 . Then, the following relation can be presented.



(a)



(b)

Fig. 3 Geometric representation of parallel OCT guide: (a) parallel guidance, (b) geometric schematic.

$$l_0 \cdot (\cos \theta_2 - \cos \theta_1) = dl/2. \quad (1)$$

From Eq. (1), it is derived that

$$\theta_2 = \cos^{-1} \left(\frac{dl}{2l_0} + \cos \theta_1 \right). \quad (2)$$

The differential expression of the vertical and horizontal motions is as follows:

$$dv = l_1 \cdot (\sin \theta_1 - \sin \theta_2), \quad (3)$$

$$dh = l_1 \cdot \left\{ \sin \theta_1 - \sin \left[\cos^{-1} \left(\frac{dl}{2l_0} + \cos \theta_1 \right) \right] \right\}, \quad (4)$$

$$dh = l_1 \cdot (\cos \theta_1 - \cos \theta_0). \quad (5)$$

In Eq. (5), horizontal motion is defined according to the control length, and it gives the control rule for the actuator to maneuver the probe in parallel. In other words, the probe could be vertically moved downward from its initial state by translating the whole frame backward, where translational motion is carried out by the active cannulas. Figure 4 shows the results of two cases, namely without control and with control.

The controlled trajectory is attained by translating the point C_1 backward, while drawing the control point C_3 in every sampling interval. The target point P_t could be vertically moved downward, so that the probe is guided to be parallel to the frontal surface. This analysis is applied to a real experiment in the same manner as that for control with the active cannulas. Other advantages of this system include its ability to generate another OCT scan in the lower side of the four-bar linkages and to acquire 3-D information about the target by rotating around the middle axis, i.e., the line connecting C_1 to C_3 , while maintaining vertical motion, i.e., spiral reconstruction of the target volume. The general procedure for measuring a sample is as follows:

1. The position and shape of the target sample is given.
2. The end-effector of the active cannulas is maneuvered to access the front of the target surface.
 - (a) The parallel guidance system is set up in the initial state.
 - (b) With the drawing and pushing of each joint, parallel scanning is performed on the sample surface.
3. After measurement, the guidance system is folded down to be inserted into the tube of the active cannulas.

4 Experiments with Biological Samples

From the design concepts and geometrical motion analysis, a laboratory prototype of the guidance system is built to double the scale. Before scanning the sample, the active cannulas are controlled such that the end-effector is located near the target, and it is assumed that the position and orientation of the sample surface are known *a priori*. In the following, the

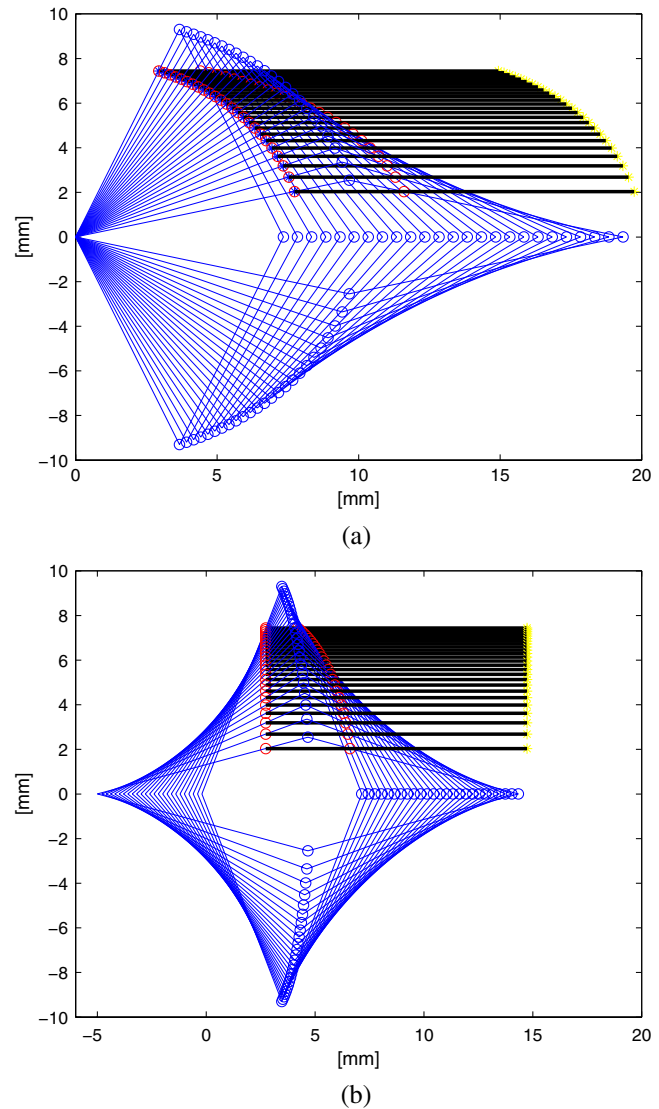
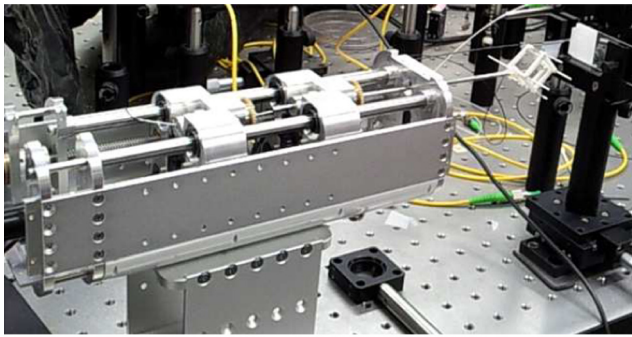


Fig. 4 Trajectories of system geometry: (a) uncontrolled trajectory, (b) controlled trajectory.

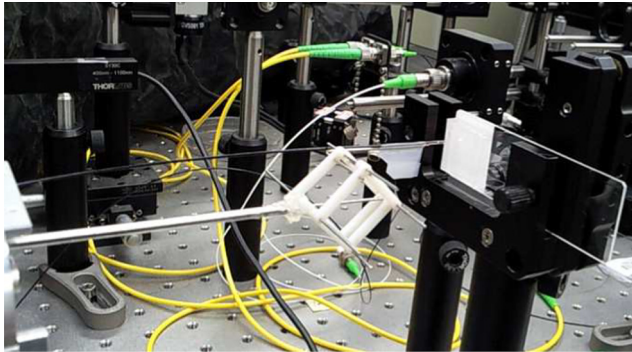
OCT fiber is inserted inside the tube of the active cannulas, and the probe is loaded into two holders of two linkages. Between the holder and the probe, some slips are allowed to not fix either support position because the probe could be broken by the moment generated at the supports. Each linkage is made up of soft plastic materials that could pass through curved tubes. Figure 5 shows the configuration of the integrated system for experiments.

To validate and calibrate the integrated system, a cover-glass sample having a flat surface and constant thickness was used. The obtained result was compared with the real value. The process was iteratively repeated until a reliable performance was attained. The result is shown in Fig. 6 where the horizontal axis shows the relative depth (A scan) in pixels and the vertical axis refers to the scan line (B scan). The relative depth is converted into the distance in μm by the refraction index and the relative pixel difference.

After calibration, the microwell plate that has regular cylinder patterns was used as a target sample for verification of the system. The sample specification and its scan result are displayed in Fig. 6. Considering the refraction index of glass



(a)



(b)

Fig. 5 Experimental setup for OCT guide system: (a) active cannulas and parallel guidance, (b) parallel guidance.

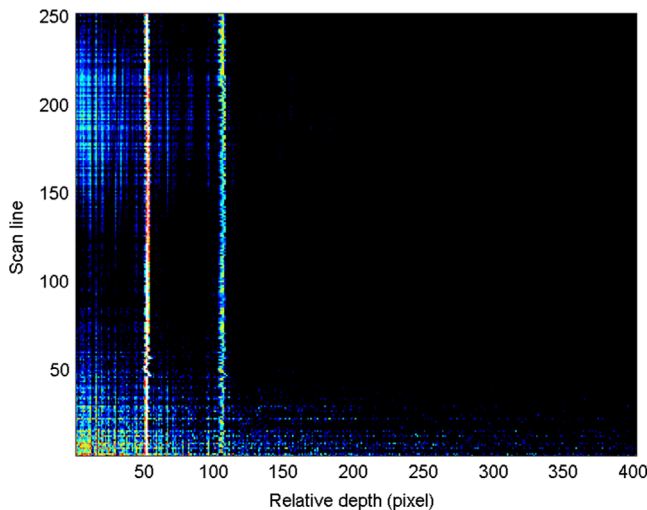
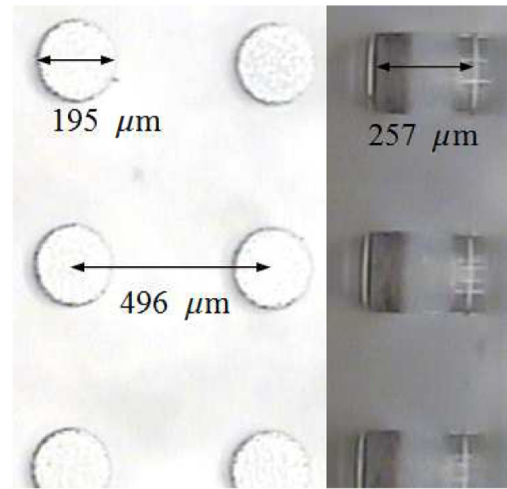
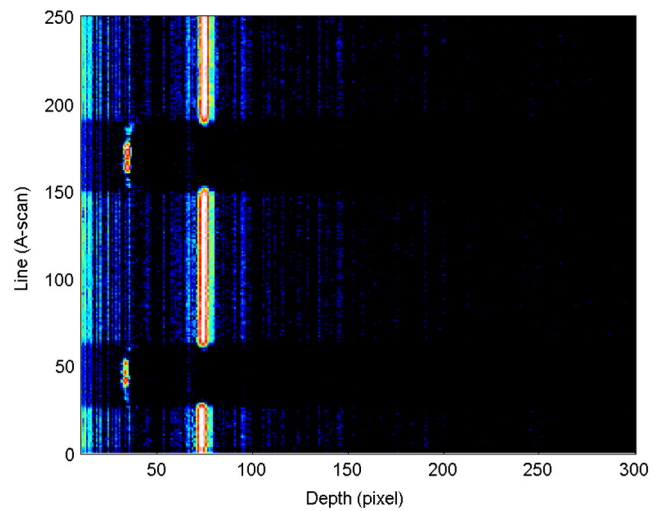


Fig. 6 Calibration result for OCT image.

as a reference sample and poly dimethylsiloxane (PDMS) as the target sample, real distances in pixels are converted and analyzed. The height difference between the two layers is 54 pixels. Using the refraction index of glass as 1.5, each pixel has a distance of $4.33 \mu\text{m}$ and the measured thickness is $234 \mu\text{m}$, while the real value is $250 \mu\text{m}$ (difference $16 \mu\text{m}$). Similarly, the target sample can be analyzed in Fig. 7. In Fig. 7, the height difference between the stepped layers is 52 pixels. Using the refraction index of PDMS as 1.4 and with each pixel having a distance of $4.64 \mu\text{m}$, the measured embossed height is $241 \mu\text{m}$ and the measured



(a)



(b)

Fig. 7 Calibration by reference sample: (a) reference sample, (b) reference measurement.

value is $257 \mu\text{m}$ (a difference of $16 \mu\text{m}$). From the result of analysis, the measurement error is 6.4% for the glass sample and 6.2% for the PDMS sample. All results show that controlled scanning ensures a reliable accuracy of less than $100 \mu\text{m}$ for diagnosis of biological samples such as tissues or cells.

In Fig. 8, two reference samples are tested for calibration of the parallel guidance in the vertical scale. The scanning probe was vertically moved from top to bottom, and its result is plotted from its axis origin. The first result displays the expanded vertical range by discriminating seven patterns which amount to a vertical range of 3 cm. Even though the guidance is double the scale of the original design, the expanded view for the inter diagnostics could considerably reduce the measurement time and the cost.

However, there are some weaknesses in the result. During 10 scans from the start, some noises could be found due to actuator start-up motions. Actually, this phenomenon is not desirable, and it could be reduced by lowering the startup acceleration with elaborate manufacturing of the mechanical parts. Another noticeable finding is that the clarity and

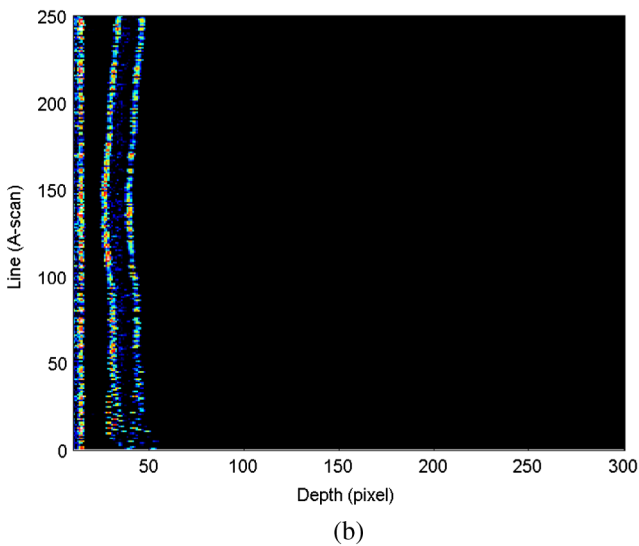
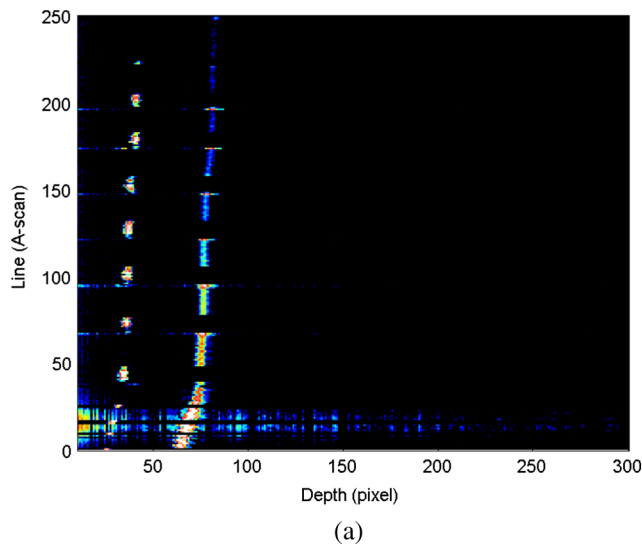


Fig. 8 Measurement result for artificial sample: (a) on Microwell plate, (b) on Scotch tape.

accuracy gets worse and this originates from the orientation changes of the probe tip due to other nonlinearities within the mechanical components. For this drawback, it is considered that roughness of the surface has a significant role in the measurement result. To compare the dependency on the roughness of the surface, a Scotch (St. Paul, Minnesota) tape was tested. As seen in Fig. 8, the case for (b) shows clearer layer boundaries than (a). From the results, it is considered that there is diffuse reflection instead of specular reflection since the tape surface is rough, and, therefore, the obtained image quality was robust to the orientation changes in the microwell plate. The result confirms the proposed measurement is effective for the measurement of most biological samples as its surface is not smooth. The pixel distance between the outer lines is $25(10 + 15)$ resulting in $146 \mu\text{m}$, and it matches well with the datasheet of the Scotch mask tape No. 214, where the thickness is $147 \mu\text{m}$.

Figure 9 shows the measurement results on some biological samples, specifically onion bark and a mouse dermis fixed on a coverglass (70–95 pixels). In Fig. 9(a), the thickness and density of the media in the bark could be acquired

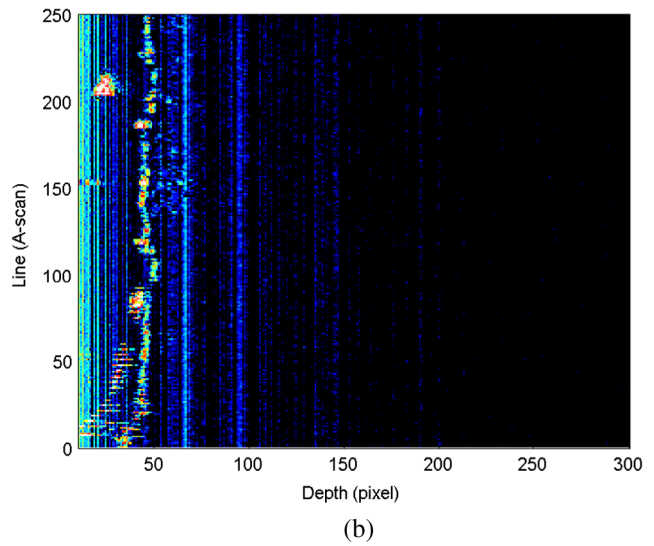
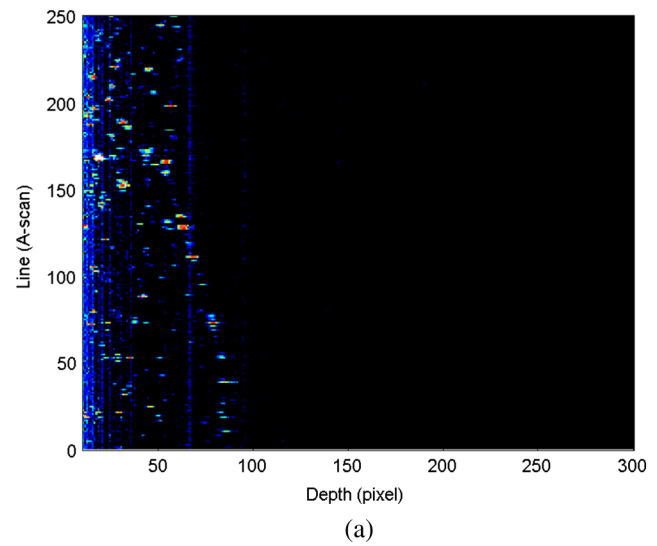


Fig. 9 Measurement results for biological samples: (a) on an onion bark, (b) on a mouse dermis.

and Fig. 9(b) also shows some information about the layers and cilia distribution.

Figure 10 presents a measurement result on the near part of retina and optic nerve in a mouse eyeball, which was described in Ref. 24. In Fig. 10(a), a part of the mouse eyeball is measured by an *in vitro* setup and Fig. 10(b) depicts its zoom-in result with the real depth scale in μm and with the same intensity pixel level (color bar) as used from Figs. 6 to 9.

Note that in all the figures displayed, the horizontal axis of the depth is converted by a corresponding refraction ratio n by scaling $6.5/n \mu\text{m}$ per each pixel. In Figs. 9 and 10, both have a scaling of $4.89 \mu\text{m}/\text{pixel}$ where n equals 1.33.

In the result, the biological information on media such as density, layers, spots, or variations of the density could be given for diagnosis. As an advantage for the system, it also has fast speed for scanning a line within only a few seconds where the speed is slowed to 35 ms in each A-scan, while still avoiding any vibration on the tip; however, its speed is faster than another comparable system as in Ref. 7. It is notable that the measurement speed for the

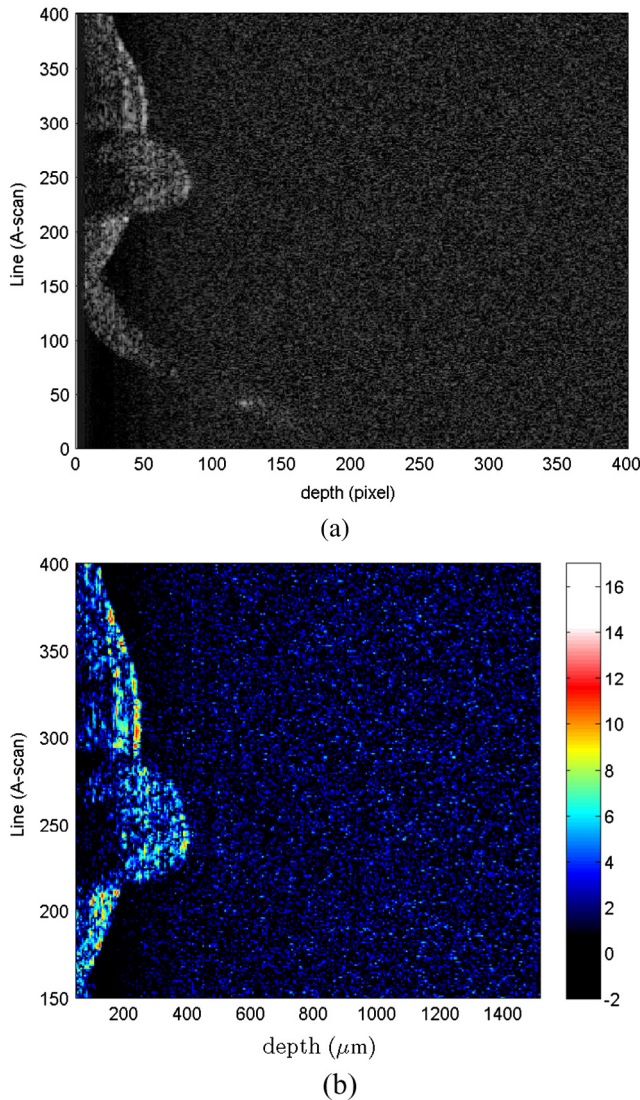


Fig. 10 Measurement results for mouse eyeball part: (a) on a mouse optic nerve, (b) magnified result.

proposed device largely depends not only on the sampling time per scan, but also on the moving speed of the parallel guidance, such that the imaging processing could be increased by the latest computing technology of multiprocessing or GPU processors while maintaining the measurement time; this could be performed as a future work.

5 Conclusions

A parallel guidance endoscopic OCT system integrated with active cannulas was proposed and a prototype was tested for procedural implementation for inspecting internal organs or complex structures accessible through small passages. The system can scan the frontal surface in parallel, and it has larger view, thus overcoming the diametrical limitation of previous endoscopic OCT systems. It also has the capability to use simultaneous scanning by dual probes on the upper and lower side linkages. By spiral scanning guidance motion, the 3-D volumetric information could be attained in a single measurement with a reduced time.

The efficient structure of the proposed system could accommodate various types of microscale operations for

physical examination, and its expanded view of internal diagnostics could considerably reduce the measurement time and cost. The system could also be used with other successive interventional operations with active cannulas such as laser ablation, biopsy, and needle insertion. More accurate pose control and increased scanning performance are required for commercial development. Also, a systematic and target media-independent performance needs to be attained in future work.

Acknowledgments

This research was supported by the KIST Institutional Program (2Z04130). The authors are also greatly thankful for eagerly working students Taeyoung Choi and Xiao Li with their elaborate experiments and consideration into the results.

References

1. A. F. Fercher et al., "Optical coherence tomography-principles and applications," *Rep. Prog. Phys.* **66**(2), 239–303 (2003).
2. J. W. Hettinger et al., "Optical coherence microscopy. A technology for rapid, in vivo, non-destructive visualization of plants and plant cells," *Plant Physiol.* **123**(13–16), 3–16 (2000).
3. A. D. Aguirre and J. F. Fujimoto, "Cellular resolution ex vivo imaging of gastrointestinal tissues with optical coherence microscopy," *J. Biomed. Opt.* **15**(1), 016025 (2010).
4. B. M. Hoeling et al., "An optical coherence microscope for 3-dimensional imaging in developmental biology," *Opt. Express* **6**(7), 136–146 (2000).
5. Z. Yaqoob et al., "Methods and application areas of endoscopic optical coherence tomography," *J. Biomed. Opt.* **11**(6), 063001 (2006).
6. G. J. Tearney et al., "In vivo endoscopic optical biopsy with optical coherence tomography," *Science* **276**(5321), 2037–2039 (1997).
7. E. Ayvali et al., "Towards a discretely actuated steerable cannula for diagnostic and therapeutic procedures," *Int. J. Robot. Res.* **31**(5), 588–603 (2012).
8. H. Yu et al., "Design, calibration and preliminary testing of a robotic telemanipulator for OCT guided retinal surgery," in *Proc. IEEE Int. Conf. on Robotics and Automation*, Karlsruhe, pp. 225–231, IEEE (2013).
9. A. D. Aguirre, "Advances in optical coherence tomography and microscopy for endoscopic applications and functional neuroimaging," Ph.D. Thesis, Massachusetts Institute of Technology (2008).
10. T.-H. Tsai, J. G. Fujimoto, and H. Mashimo, "Endoscopic optical coherence tomography for clinical gastroenterology," *Diagnostics* **4**(2), 57–93 (2014).
11. T. Just et al., "Optical coherence tomography as a guide for cochlear implant surgery?," *Proc. SPIE* **6842**, 68421F1 (2008).
12. L. A. Kahrs, T. R. McRackan, and R. F. Labadie, "Intracochlear visualization: comparing established and novel endoscopy techniques," *Otol. Neurotol.* **32**(9), 1590–1595 (2011).
13. A. Podoleanu et al., "Three dimensional OCT images from retina and skin," *Opt. Express* **7**(9), 292–298 (2000).
14. C. Hitzenberger et al., "Three-dimensional imaging of the human retina by high-speed optical coherence tomography," *Opt. Express* **11**(21), 2753–2761 (2003).
15. B. Baumann et al., "Total retinal blood flow measurement with ultra-high speed swept source/Fourier domain OCT," *Biomed. Opt. Express* **2**(6), 1539–1552 (2011).
16. S. A. Boppart et al., "Forward-imaging instruments for optical coherence tomography," *Opt. Lett.* **22**(21), 1618–1620 (1997).
17. M. R. Hamblin and T. N. Demidova, "Mechanisms of low level light therapy," *Proc. SPIE* **6140**, 614001 (2006).
18. J. Burgner et al., "A bimanual teleoperated system for endonasal skull base surgery," in *Proc. IEEE/RSS Int. Conf. on Intelligent Robots and Systems*, San Francisco, CA, pp. 2517–2523, IEEE (2011).
19. R. J. Webster, J. M. Romano, and N. J. Cowan, "Mechanics of pre-curved-tube continuum robots," *IEEE Trans. Robot.* **25**(1), 67–78 (2009).
20. K. Zhang et al., "A surface topology and motion compensation system for microsurgery guidance and intervention based on common path optical coherence tomography," *IEEE Trans. Biomed. Eng.* **56**(9), 2318–2321 (2009).
21. R. J. Webster et al., "Nonholonomic modeling of needle steering," *Int. J. Robot. Res.* **25**(5), 509–525 (2006).
22. P. Sears and P. E. Dupont, "Inverse kinematics of concentric tube steerable needles," in *Proc. IEEE Int. Conf. on Robotics and Automation*, Roma, pp. 1887–1892, IEEE (2007).

23. P. E. Dupont et al., "Design and control of concentric tube robots," *IEEE Trans. Robot.* **26**(2), 209–225 (2010).
24. L. M. Sakata et al., "Optical coherence tomography of the retina and optic nerve: a review," *Clin. Exp. Ophthalmol.* **37**(1), 90–99 (2009).

Suhyeon Gim received his BS and MS degrees in mechanical engineering from Korea University in 2001 and 2003, and his PhD degree in robotics from Mokwon University in 2009 through KAIST course completion. He worked at KIST in 2013 on this topic and is currently with Institut Pascal in France on the research of path planning with robotics control. His research interests include safe trajectory planning for vehicle autonomy or needle steering and surgical robotics.

Hyowon Moon received his BS and MS degrees in electrical engineering from Seoul National University, Seoul, Republic of Korea, in 2010 and 2012, respectively. He joined KIST in 2012, where he is currently a research scientist. His research interests include optical fiber sensors, fiber Bragg gratings, and biomedical imaging.

Hyun-Joon Shin received his PhD degree in physics from Korea Advanced Institute of Science and Technology (KAIST), Republic of Korea, in 2000. Currently he is working as a principal research scientist at KIST. His research interests include optical bioimaging systems and optogenetics.

Deukhee Lee is a senior researcher in the Center for Bionics at KIST. His research interests include the study of surgical navigation and ultrasonic diagnosis and therapeutics. He received his BS degree from Hanyang University in mechanical engineering, his MS degree from Seoul National University in mechanical engineering, and his PhD degree in mechanical engineering from the University of Tokyo.

Sungchul Kang received his BS, MS, and PhD degrees in mechanical engineering from Seoul National University, Seoul, Republic of Korea, in 1989, 1991, and 1998, respectively. In 1991, he joined KIST, where he is currently a principal research scientist. His research interests include robot manipulation, haptic sensing and display, field robot systems, and medical robotics.

Keri Kim received her BS degree in mechanical engineering from Seoul National University, and her MS and PhD degrees in mechano-informatics from the University of Tokyo. Currently she is working as a senior research scientist in the Center for Bionics at KIST. Her research interests include endoscopic instruments and medical robotics.